Small-Angle Neutron Scattering of a Solvent-Swollen Segmented Polyurethane as a Probe of Solvent Distribution and Polymer Domain Composition

Joseph T. Mang,[†] Rex P. Hjelm,*[,‡] E. Bruce Orler,[§] and Debra A. Wrobleski[§]

Dynamic Experimentation Division, Los Alamos National Laboratory, Los Alamos, New Mexico 87545; Manuel Lujan, Jr. Neutron Scattering Center, Los Alamos National Laboratory, Los Alamos, New Mexico 87545; and Materials Science and Technology Division, Los Alamos National Laboratory, Los Alamos, New Mexico 87545

Received January 3, 2008; Revised Manuscript Received March 31, 2008

ABSTRACT: Segmented polyurethanes consist of alternating rigid aromatic (hard) and flexible (soft) segments that phase separate into hard and soft segment-rich nanodomains. The domain structure results in what has been presumed to be an extended, cross-linked network, giving these materials unique mechanical properties. Because of poor contrast and volume fractions of the discontinuous phase, previous scattering studies have focused on polyurethanes with hard segment contents greater that 30 wt %. This study focused on a commercial poly(ester urethane), Estane 5703, containing only 23 wt % hard segment content. To probe the domain structure and composition, we used small-angle neutron scattering (SANS) with contrast variation methods on bulk samples swollen with deuterated/protonated mixtures of benzene, toluene, or *o*-, *m*-, or *p*-xylene isomers. We used the fluid model and Pedersen's micelle model to describe the SANS data as a function of contrast. Both the fluid and micelle models consider Estane as a fluid of spherical, discrete domains in a soft segment-rich matrix. The discrete domains have a closest center-to-center approach defined by the Percus−Yevick hard-sphere potential. The micelle model divides the discontinuous domain into a core and a surrounding corona. We find that the micelle model completely described the data, whereas the fluid model required the ad hoc addition of an additional length scale. The models, which were in good agreement with each other, show that in Estane the discrete domains comprised a small fraction, 0.05−0.06, of the sample volume and have a radius of about 5 nm, giving a number density of the order 10^{17} cm^{-3}. Furthermore, the discrete domains contain a higher hard segment concentration than the matrix, but incorporated only 0.06−0.13 of the hard segment volume. The results also show there is considerable mixing of the hard and soft segments, and there is a significant amount of soft segment in the discrete domains. Using these results, we were able to determine some important factors behind the thermomechanical properties of Estane. Furthermore, we make a critical assessment of the view that the discrete domains are cross-links for a continuous network and forward the hypothesis that the domains are more like filler particles coupled to the matrix by polymer entanglements.

1. Introduction

Thermoplastic polyurethanes derive their unique mechanical properties from the thermodynamic incompatibility of low glass transition temperature, T_g, soft segments with covalently attached hard segments.[1−19] Phase separation of the hard and soft segments into hard and soft segment-rich nanoscale domains creates a material that has very high stress to break and toughness.[2,3,5] Since the hard segments on different chains are not chemically bound, these materials are thermoplastic above the hard segment T_g or melting temperature. When the polymer is cooled below the hard segment T_g, the hard segments phase separate and, according to the prevalent view, re-form the network. The rate of this supposed network re-formation and degree of phase separation have been directly correlated with the tensile properties of polyurethane elastomers.[10,20] Thermoplastic polyurethanes represent an important class of segmented copolymers.

Segmented copolymers represent an intermediate system between random and block copolymers. In contrast to block copolymers that typically contain two or three blocks with molecular weights in excess of 5000 Da, segmented copolymers have multiple segments with lengths between 500 and 5000 Da along the polymer backbone. The phase segregation of short segments of segmented polyurethanes is constrained by their mobility, connectivity, and thermodynamic interaction. Thus, segmented polyurethanes cannot form highly order equilibrium morphologies, unlike block copolymers, making morphological characterization challenging. While the general effects of phase separation on the mechanical properties of segmented polyurethanes are accepted as depending on the number, shape, size, distribution, interfacial bonding of the hard and soft segment-rich domains, and mixing of the hard and soft segments, the details of the structure−property relationships, phase morphology, and phase behavior of these complex materials are not well understood.

It is well established by work on polyether-based polyurethanes with methyldiphenyl diisocyanate (MDI) hard segments with butanediol (BDO) chain extender that the phase separation of the hard and soft segments is not complete. The degree of phase separation has been raised repeatedly as important to properties of segmented polyurethanes: domain composition is interrelated with the domain structure, and therefore, it is essential to understanding the material mechanical properties. Consequently, considerable effort has gone into characterizing the extent of phase separation.[3,7,12,21] Information on the domain compositions also is useful to determine the thermodynamic parameters that drive equilibrium phase segregation. Overall, this type of information will provide a basis for predicting the performance of multiphase polymers.

* Corresponding author: Tel 505-665-2372, Fax 505-665-2676, e-mail hjelm@lanl.gov.
[†] Dynamic Experimentation Division.
[‡] Manuel Lujan, Jr. Neutron Scattering Center.
[§] Materials Science and Technology Division.

10.1021/ma800015g CCC: $40.75
Published on Web 05/30/2008

The subject of this study is a commercial segmented poly(esterurethane) with low, 23 wt %, hard segment content, Estane. One of the difficulties in determining domain structure of segmented polyurethanes with low hard segment content and where there is weak segregation of hard and soft segments is the experimental difficulty of "seeing" domain structure. The small volume fractions and weak contrast of the discrete domains in these materials make visualization almost impossible by conventional microscopy and scattering techniques. Consequently, previous work, with a few exceptions, has focused on either strongly segregated, segmented polyurethanes or, in the case of weakly segregating polyurethanes, those containing no less than 30 wt % hard segment content.[3,4,12,14–16,18,19,22–25] These higher hard segment content materials exhibit nanophase order at length scales of around 10 nm and segregation characteristics that make them more amenable to scattering studies. Studies of segmented polyurethanes with lower hard segment content, however, are very important due to their applications as adhesives and binders. There is additional motivation for the study these materials to obtain additional information on the structure−property relationships of polyurethanes as a class.

In order to develop more robust mechanical models for segmented copolymers, much greater details of the morphology must be obtained. While there have been a few of SANS studies on segmented polyurethanes,[14,15] this technique has not been fully utilized. The principal strength of SANS is the increased scattering that can be manipulated by isotopic substitution of deuterium for hydrogen. The combination of swelling and scattering from contrast variation experiments has a sound fundamental basis since solvent swelling experiments have been commonly used in polymer physics for assessing the thermodynamics of mixing and characterization of polymer networks, including those of polyurethanes.[21,26–32] In addition, the analysis of data using contrast variation techniques is well understood.[33–35] Early work by Nierzwick and Majewska pointed out that such studies could even give information on polyurethane domain composition.[21]

The objective of this work was to use swelling with solvents that are mixtures of protonated and deuterated forms of either benzene, toluene, or one of the xylene isomers as a contrast variation technique with SANS as a means of determining the size, shape, solvent distribution, and composition of the different domains in a low, 23 wt %, hard segment content polyurethane, Estane. Thus, we expanded on earlier attempts to study domain morphology and composition with SANS measurements of polyurethanes with deuterated soft segment[14,15] and X-ray[12,16,24,25] measurements on higher hard segment content polyurethanes. This approach was necessary in the study of commercial polyurethanes, as deuterated model compounds that might otherwise be used in this type of study are not necessarily completely equivalent to the actual product.

We found that Estane consists of discrete domains with relatively higher hard segment content than the embedding continuous matrix. Furthermore, we found that there is incomplete segregation of hard and soft segments. Using statistical arguments and the notion that in segmented polyurethanes a minimum size of hard segment block is required for incorporation into the discrete domains,[3,7,12] we made an assessment of the alternate views that either the discrete domains act as junctions of an extended network or that they act as filler particles. We advanced the hypothesis that the discontinuous domains act as filler particles dynamically coupled with the matrix by entanglements. We also explored the plausibility of using the swelling data with the contrast variation technique to estimate the thermodynamics of swelling of a polymer with complex domain structure, such as polyurethane, and explore further the relationships among swelling thermodynamics, structure, and mechanical properties.

2. Experimental Section

2.1. Materials. Estane 5703, obtained as pellets from The BF Goodrich Co., contains ~23 wt % hard segments composed of 4,4′-methylenediphenyl 1,1′-diisocyanate (MDI) and a 1,4-butanediol (BDO) chain extender. The soft segments are comprised of 1000 Da poly(butylene adipate).[36,37] The chemical structures of the Estane components are given in ref 37. Protonated benzene, toluene, and *o*-, *m*-, and *p*-xylene as well as deuterated benzene-d_6, toluene-d_8, and *o*-, *m*-, and *p*-xylene-d_{10} were obtained from Aldrich and were used as received.

2.2. Determination of Molecular Weight Distribution. Gel permeation chromatography (GPC) was used to determine molecular weight distributions of Estane 5703. The GPC consisted of an Alliance 2690 pump equipped with a Wyatt Rex differential refractive index detector and utilized three Polymer Laboratories PL Mixed B GPC columns at 70 °C (DMF)) at a flow rate of 1.0 mL min^{-1}. The molecular weight distribution for polyester urethanes is best characterized by using polyethylene oxide standards in DMF as demonstrated by previous work through absolute molecular weight measurements using vapor phase osmometry for M_n and using multiangle light scattering for M_w.[38] The molecular weights were calculated relative to the retention times of poly(ethylene oxide) standards for DMF using Empower software. The molecular weights of Estane 5703 are M_n = 45 kDa, M_w = 81 kDa, M_z = 131 kDa, and $M_w/M_n \equiv \mathrm{PD} = 1.8$.

2.3. Estane Film Preparation. Estane pellets were compression-molded into 0.5−1.0 mm thick films using a hydraulic press (Carver) with heated platens. The pellets were preheated to 110 °C for 5 min before pressing. After being pressed at 42 MPa, 110 ± 1 °C for 5 min, the films were rapidly cooled to room temperature. To allow for equilibration of the morphology, the films were held at room temperature for 1 year before swelling and characterization by SANS.

2.4. Swelling. Estane disks 12.5 mm in diameter were cut and swollen in benzene, toluene, *o*-xylene, *m*-xylene, or *p*-xylene containing 0, 0.25, 0.5, 0.75, or 1.0 volume fraction, f_D, of perdeuterated solvent. Generally, the samples reached a stead-state solvent uptake within 4 h. The swelling results were reported after 48 h of exposure, well after there was no additional weight increase for any of the solvents. The volume fractions of solvent uptake given in Table 1 were assumed to be at equilibrium.

2.5. Small-Angle Neutron Scattering. Small-angle neutron scattering measurements were performed on the time-of-flight, low-Q diffractometer, LQD, at the Manuel Lujan Jr. Scattering Center. Swollen samples were placed, with solvent, in cells fabricated of fused silica designed with ground glass closures. The cells were designed to eliminate solvent evaporation and ease handling of the swollen films. The path lengths of the cells were 2 mm for solvent mixtures with f_D greater than 0.5 and 1 mm with solvent mixtures with f_D less than or equal to 0.5.

Data were reduced by conventional methods[39,40] to an absolute scale, differential scattering cross section per unit volume, $d\Sigma(Q)/d\Omega$ (cm^{-1}), as a function of momentum transfer, $Q = 4\pi/\lambda \sin\theta$, where 2θ is the scattering angle and λ is the incident neutron wavelength. Scattering intensities were corrected for solvent background by determining the volume fraction of solvent in the swollen Estane films and subtracting the appropriate fraction of the measured solvent scattering intensity from that of the swollen films.

3. Theoretical Section

Initial assessment of the SANS data indicated that the hard segment-rich phase formed into discrete domains embedded in a soft segment-rich matrix. This paper uses two models, the fluid and micelle models, summarized in Figure 1, to analyze the scattering data. The models differ in the treatment of the discrete hard segment-rich domain structure. The fluid model

Table 1. Scattering Length Densities of Estane and Solvents and Swelling Data

component		volume fractions, ϕ_i, in swollen Estane[a] hard segment, ϕ_H	soft segment, ϕ_S	solvent, ϕ_{sol} calculated	measured	ρ (10^{10} cm^{-2}) protonated	deuterated	δ^b (MPa)$^{0.5}$
neat Estane	hard segment	0.20				2.7		23.5[c]
	soft segment		0.80			1.1		19.7
swelling solvent	benzene	0.0749	0.295	0.630	0.60	1.2	5.4	18.8
	toluene	0.107	0.404	0.489	0.46	0.94	5.7	18.2
	o-xylene	0.113	0.441	0.447	0.41	0.78	5.9	18.5
	m-xylene	0.125	0.488	0.387	0.36	0.78	5.9	18.1
	p-xylene	0.126	0.497	0.377	0.35	0.78	5.9	18.0

[a] Volume fractional uptakes measured after 48 h. However, volumes do not change after 4 h. [b] Solubility parameters, δ. Solvent values taken from ref 48. [c] Solubility parameter for hard segment from ref 59. Also see ref 58.

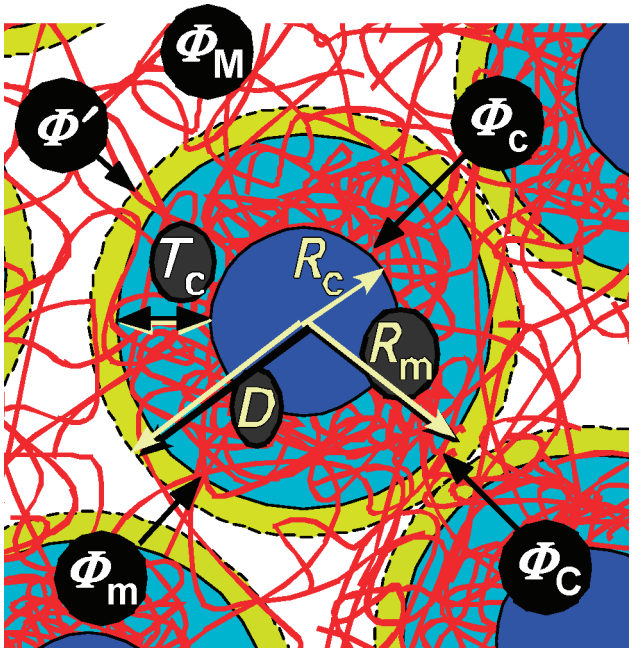

Figure 1. Schematic of the fluid and micelle models used in the analysis of SANS data. In both models discrete domains are embedded in a continuous matrix. In the micelle model the discrete domains consist of a core (dark blue) with radius R_c and a corona (light blue) of thickness, T_C. Each domain has an overall radius, R_m. A hard-sphere interaction (yellow) distance, D, is assumed to exist, which prevents the discrete domains from having a center-to-center distance less than $2D$. The fluid model is distinguished from the micelle model by having a homogeneous discrete domain. The discrete domain and continuous matrix take up respective volume fractions $\Phi_m = 1 - \Phi$ and $\Phi_M = \Phi$. In the micelle model the volume fractions of the core and corona are represented as Φ_c and Φ_C, respectively. The volume fraction occupied by the hard sphere interaction is Φ'. The boundaries of the spherical domains defining each of these volume fractions are pointed by the arrows. The volume factions of hard and soft segments and the solvents over the entire sample are given by ϕ_H, ϕ_S, and ϕ_{sol}, respectively. The compositions of the different domains are given by the symbols, φ_{ij}, where i is one of the domains, M or m for the matrix or discrete domain of the fluid and micelle models, and c or C for the core or corona of the micelle model. The index j refers to the components, H, for hard segment, S, for soft segments and, Sol, for solvent. The same symbols with primes indicate the corresponding value corrected for the volume of solvent swelling, with the exception of Φ'.

envisions the domains as spheroids of revolution with an average radius, R, and with a hard-sphere-like interaction potential at distance, D, from the sphere center. The fluid model has been used previously to analyze small-angle X-ray (SAXS) data from other low hard segment content polyurethanes.[24,25] The micelle model, derived by Pedersen,[41,42] treats the structure of the discrete domains as a uniform core, surrounded by a corona of hard segment intermixed with the matrix. The micelle model has proved successful in describing the structure of micelles of block copolymers[42] and polymer-modified surfactants in solution.[43]

The fluid model assumes that the swollen Estane consists of spheroid domains that have a different chemical composition from the matrix in which they are embedded. The two length scales of the fluid model, R and D, are derived from $d\Sigma(Q)/d\Omega$ using the relationship

$$\frac{d\Sigma(Q)}{d\Omega} = NV^2\Delta\rho^2 P(R,Q)\, S(D,\Phi',Q) + B(Q) \qquad (1)$$

where $P(R,Q)$ is the spherical particle form factor

$$P(R,Q) = |F(R,Q)|^2; \quad F(R,Q) = \left[3\,\frac{\sin QR - QR\cos QR}{(QR)^3}\right] \qquad (2)$$

$S(Q)$ is the structure factor, describing the particle interactions, V is the particle volume, and N is the particle number density. $S(Q)$ is calculated assuming hard-sphere interactions for the descrete domains using the Percus−Yevick model[44,45] and gives the hard-sphere interaction radius, D. According to this model, discrete domains cannot have a center-to-center distance of less than $2D$ apart. The volume fraction of the spheroid region defined by D, Φ', was determined from $S(Q)$. The volume fraction of the domain that contrasts with the matrix was then determined as

$$1 - \Phi = (R/D)^3\Phi' \qquad (3)$$

where Φ is the volume fraction of the matrix. The background term, $B(Q) = A\exp(-aQ)$, accounts for residual sample inhomogeneity, such as voids, and any internal and domain interfacial structure of the spheres not accounted for by the fluid model.

The contrast between the discrete domains, m, and the matrix, M, $\Delta\rho = \rho_m - \rho_M$, was calculated from the Porod invariant

$$Q_p = \int_0^\infty Q^2\,\frac{d\Sigma(Q)}{d\Omega}\,dQ = 2\pi^2\Phi(1-\Phi)\Delta\rho^2 \qquad (4)$$

The invariant, eq 4, was computed from the SANS data after subtraction of $B(Q)$.

In the micelle model the form factor is given by

$$F_{mic}(Q) = V_{core}{}^2\Delta\rho_{mM}{}^2P(R,Q) + N_{agg}V_{ch}{}^2\Delta\rho_{crM}{}^2F(R_g,Q) + 2N_{agg}V_{core}V_{ch}\Delta\rho_{mM}\Delta\rho_{crM}S_{cch}(R,R_g,Q) + N_{agg}(N_{agg}-1)V_{ch}{}^2\Delta\rho_{crM}{}^2S_{chch}(R,R_g,Q) \qquad (5)$$

where the subscript cr refers to the corona, V_{core} is the volume of the micelle core, V_{ch} is the volume of a chain in the corona, N_{agg} is the aggregation number of the micelle, and $F(R_g, Q)$ is the Debye equation for single chain scattering from a Gaussian coil.[42] $S_{cch}(R,R_g,Q)$ and $S_{chch}(R,R_g,Q)$ are functions describing core−chain and chain−chain correlations, respectively:[42]

$$S_{\mathrm{chch}}(R, R_{\mathrm{g}}, Q) = \psi(R_g, Q)^2\left[\frac{\sin(Q[R+R_{\mathrm{g}}])}{Q[R+R_{\mathrm{g}}]}\right]^2$$

$$\psi(R_{\mathrm{g}}, Q) = \frac{1-\mathrm{e}^{-(Q^2R_{\mathrm{g}}{}^2)}}{Q^2R_{\mathrm{g}}{}^2}$$

$$S_{\mathrm{cch}}(R, R_{\mathrm{g}}, Q) = F(R, Q)\ \psi(R_{\mathrm{g}}, Q)\frac{\sin(Q[R+R_{\mathrm{g}}])}{Q[R+R_{\mathrm{g}}]}$$

Because of the complexity in the form factor, the total scatter given in eq 1 does not apply to the micelle model; rather, a decoupling approximation must be made:[42]

$$I_{\mathrm{mic}}(Q) = N[F_{\mathrm{mic}}(Q) + A_{\mathrm{mic}}{}^2(Q)(S(D, \Phi', Q) - 1)] \quad (6)$$

In the above expression, N is the particle density, as before, and $A_{\mathrm{mic}}(Q)$ results from the decoupling approximation and is given by[42]

$$A_{\mathrm{mic}}(Q) = V_{\mathrm{core}}\Delta\rho_{\mathrm{mM}}F(R, Q) + N_{\mathrm{agg}}V_{\mathrm{ch}}\Delta\rho_{\mathrm{crM}}\psi(R_{\mathrm{g}}, Q)\frac{\sin(Q[R+R_{\mathrm{g}}])}{Q[R+R_{\mathrm{g}}]} \quad (7)$$

The contrast terms, $\Delta\rho_{\mathrm{mM}}$ and $\Delta\rho_{\mathrm{crM}}$, for the micelle model (eqs 5 and 7) were calculated by simultaneously fitting the data (for a given solvent) at all f_{D}.

Having made estimates of R and $1 - \Phi$ for either the fluid or micelle models, the number density of spheroid domains can be determined from eq 1 as

$$N = 3\,\frac{1-\Phi}{4\pi R^3} \quad (8)$$

The composition of the discrete domains and the matrix phase was computed from the measured sample compositions and $\Delta\rho$ using

$$\Delta\rho = \sum \rho_i\phi_{i\mathrm{m}} - \sum \rho_i\phi_{i\mathrm{M}} \quad (9)$$

and

$$\phi_i = \sum \phi_{ij}\Phi_j \quad (10)$$

along with the condition that the sums of the various volume fractions must be unity. In eqs 9 and 10, ρ_i is the scattering length density of the ith component (either hard segment, H, soft segment, S, or solvent, sol), and ϕ_{ji} is the volume fraction of i in the jth domain or phase (either m or M or c for core and C for corona in the micelle model), Φ_j is the volume fraction of the jth domain, and ϕ_i is the total volume fraction of i in the sample. The latter was determined from the known chemical composition of the Estane and the amount of solvent taken up in the equilibrium swelling (Table 1). In our model calculations we assumed that the scattering length densities of the hard segments were an average of the molar content of BDO and MDI in Estane, 0.2 and 1.2, respectively. The soft segment scattering length density was calculated from the adipate composition. The total scattering length density of Estane was then computed from the molar ratio of adipate monomer (an average of five in the 1 kDa oligomer) to BDO to MDI, 5:0.2:1.2. The ϕ_{ji} for the micelle model were determined by simultaneous fits of the data at all contrasts, whereas the ϕ_{ji} for the fluid model were determined by the following analysis of the Porod invariant.

It is straightforward to show that a plot of the square root of Q_{p}, (eq 4), vs the solvent scattering length density, ρ_{sol}, is a straight line, by replacing $\Delta\rho$ in eq 4 with eq 9, keeping in mind that the sign of the square root will be negative when the average scattering length of the matrix, ρ_{M}, including the solvent, is greater than that of the discrete domains, ρ_{m}. The slope of the line, s, and the $Q_{\mathrm{p}} = 0$ intercept, $\bar{\rho}$, for the a plot of $\sqrt{Q_{\mathrm{p}}}$ vs ρ_{sol} are

$$s = \sqrt{\frac{1-\Phi}{\Phi}}(1 - \varphi_{\mathrm{sol}} - \phi_{\mathrm{Hm}} - \phi_{\mathrm{Sm}}) \quad (11)$$

and

$$\bar{\rho} = \frac{(\varphi_{\mathrm{S}} - \phi_{\mathrm{Sm}})\rho_{\mathrm{S}} + (\varphi_{\mathrm{H}} - \phi_{\mathrm{Hm}})\rho_{\mathrm{H}}}{1 - \varphi_{\mathrm{sol}} - \phi_{\mathrm{Hm}} - \phi_{\mathrm{Sm}}} \quad (12)$$

We now have two equations and two unknowns, ϕ_{Sm} and ϕ_{Hm}. This approach provides a convenient method for determining the two partial volume fractions, ϕ_{Sm} and ϕ_{Hm}. The values obtained from this procedure were used to determine the remaining values using eqs 9 and 10, using the various known volume fractions in Table 1.

The difference between earlier attempts to determine the domain compositions in polyurethanes,[12,24] and this work is solvent swelling. The ability to change ρ_{sol} through the use of the strong difference in scattering between deuterated and protonated swelling agents was essential to this approach. The change in contrast afforded by this technique provides the additional dimension required, through eqs 9, 10, 11, and 12, to determine the discrete domain and matrix compositions. This approach, which has formal similarities to the contrast variation method developed for structural biology[46,47] and later applied to polymer composites,[33–35] was not available to the SAXS studies.

4. Results and Analysis

4.1. Swelling with Benzene, Toluene, and *o*-, *m*-, and *p*-Xylene. Estane retained its mechanical integrity when swollen to equilibrium with benzene, toluene, or either of the xylene isomers, suggesting that the physical structure is retained. This was consistent with the observation of other polyurethanes that swelling by these solvents had a small effect on the tensile strength.[32] Table 1 summarizes the volume fraction uptake of benzene, toluene, and *o*-, *m*-, and *p*-xylene at equilibrium after 48 h swelling. Calculated values from the weight uptake measurements (assuming ideal mixing) and measured volume increases are shown. The measured volume changes are systematically smaller than the calculations based on ideal mixing. However, the differences are small, 5−8%, and within the likely errors of the volume measurements. So, while there may be evidence for nonideal mixing, we used the ideal mixing assumption (Table 1) to compute the volume fractions derived from the SANS (Figure 2). The differences between the

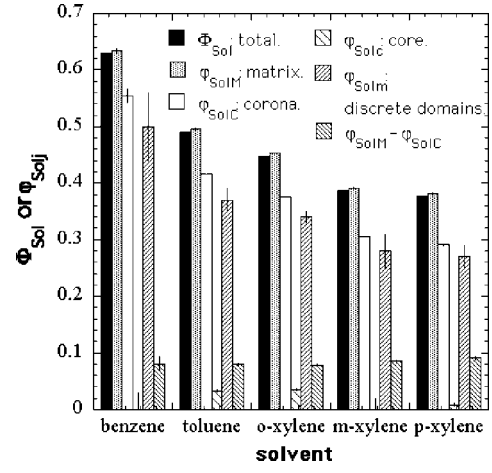

Figure 2. Total volume fractions of solvent and solvent volume fractions in different domains of Estane swollen with different agents. Vertical bars indicate standard deviations.

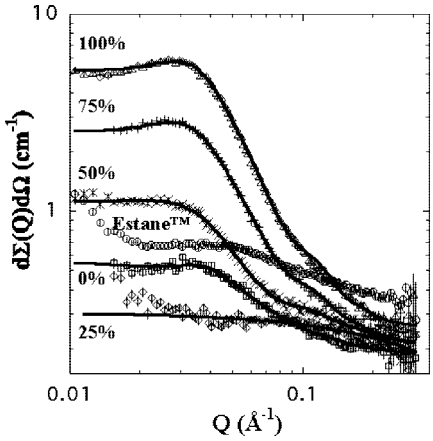

Figure 3. SANS of Estane neat and swollen with mixtures of deuterated and protonated toluene and comparison of the data with the fluid model: Data: (○) neat Estane; Estane swollen in (□) $f_D = 0$, (◇) $f_D = 0.25$, (×) $f_D = 0.50$, (+) $f_D = 0.75$, and (△) $f_D = 1.0$. Small, vertical lines indicate the value of the standard deviation of the intensity data. Lines show the results of calculations for the fluid model.

measured and calculated volume fractions did not affect the results in any substantial way.

The amount of solvent in the swollen sample decreased with the number of methyl groups on the aromatic ring and with the relative positions of xylene methyl groups. Swelling decreased in the order *o-, m-*, and *p*-xylene (Table 1, Figure 2), suggesting that steric factors play a role in the swelling of Estane by these solvents. Furthermore, with the exception of toluene, the amount of swelling increased as solubility potentials, δ, of the solvents (as determined by Hoy[48]) increased toward that of BDO (Table 1).

Figure 3 shows the SANS intensity from neat Estane and Estane swollen with toluene mixtures having different f_D. Neat Estane shows a scattering peak with a broad maximum centered at $Q \approx 0.04$ Å^{-1}. This result was consistent with phase-sensitive tapping mode AFM images of Estane[49] and other polyurethanes with low hard segment content,[16] all of which showed a structure with small, discrete domains, having dimensions of order 10 nm, which appear slightly harder than the surrounding matrix.

Swelling with toluene resulted in a shift of the peak to smaller $Q \approx 0.03$ Å^{-1}, reflecting an increase in spacing between the discrete domains due to extensions of the soft segments by swelling. The scattering intensity of the swollen Estane samples decreased as f_D was increased from 0 to 0.25 (Figure 3), indicating a decrease in the contrast between the Estane structural elements as f_D was increased over this range. The scattered intensity then increased as the volume fraction of d-toluene was increased from $f_D = 0.5-1.0$, indicating an increase in contrast between structural elements as f_D was increased to larger values.

The results from the *o-*, *m-*, and *p*-xylene contrast series were very similar to those for the toluene contrast series (Figure 4a−c). However, there were significant differences in the peak heights. This was particularly noticeable in the sample swollen in $f_D = 1.0$ d-xylene, where the peak became less intense in the sequence *o-*, *m-*, and *p*-xylene. Furthermore, there was a change in the relative intensities of samples swollen in $f_D = 0$ and 0.5 in the case of *p*-xylene (Figure 4c).

SANS of Estane swollen with benzene (Figure 5) showed similar behavior as observed with the other solvents. The intensities for $f_D = 0$ and 0.25 were almost the same, and the intensity of the scattering peak at larger values of f_D was of greater magnitude than observed with the other solvents. However, the scattering peak was less distinct in the benzene-

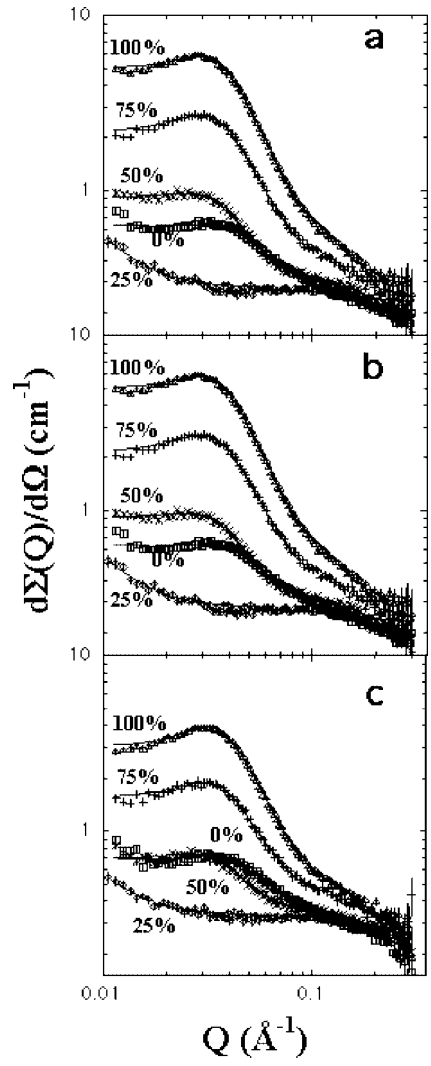

Figure 4. SANS of Estane swollen with mixtures of deuterated and protonated *o-*, *m-*, and *p*-xylene and comparison of the data with the fluid model: (a) *o*-xylene; (b) *m*-xylene; (c) *p*-xylene. Data: Estane swollen in (□) $f_D = 0$, (◇) $f_D = 0.25$, (×) $f_D = 0.50$, (+) $f_D = 0.75$, and (△) $f_D = 1.0$. Small, vertical lines indicate the value of the standard deviation of the intensity data. Lines show the results of calculations for the fluid model.

swollen samples, suggesting greater mixing of the solvent with the discrete domains.

The analyses described below showed that these observations are consistent with the presence of discrete hard segment-rich domains embedded in a continuous soft segment-rich matrix phase. The differences in the SANS data with f_D that occurred with different solvents were due to the amount of swelling by the solvent. When Estane is swollen with benzene, toluene or any of the xylene isomers, the swelling is largely confined to the matrix phase that is rich in soft segments. Benzene swelled the continuous phase to a greater degree than the other solvents. This observation was not entirely surprising since the solubility parameter of benzene is closest to that estimated for the soft segments (Table 1).

4.2. Fluid Model Analysis. For the fluid model, the data for each contrast series for each solvent were fit separately, allowing all structure parameters to vary freely, except for the matrix volume fraction, Φ, which was set from the determination of $S(Q)$ and eq 3. The scattering below $Q = 0.01$ Å^{-1} was not reproducible from one sample to the next. Thus, we assumed that for low Q the scattering curve does not reflect the Estane domain structure; rather, it was due to process-dependent

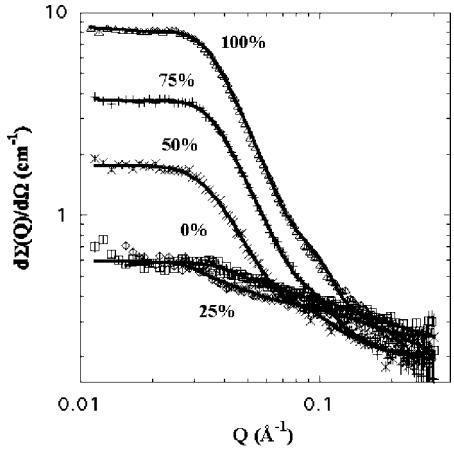

Figure 5. SANS of Estane swollen with mixtures of deuterated and protonated benzene and comparison of the data with the fluid model: Data: Estane swollen in (□) $f_D = 0$, (◇) $f_D = 0.25$, (×) $f_D = 0.50$, (+) $f_D = 0.75$, and (△) $f_D = 1.0$. Small, vertical lines indicate the value of the standard deviation of the intensity data. Lines show the results of calculations for the fluid modes.

nonhomogeneities, and we discounted it, treating it as background intensity, as discussed above (eq 1). Contrast variation analysis for the fluid model was done using eqs 11 and 12. Because the Q_p is proportional to the total squared contrast-weighted product of the phase volume factions (eq 4), the necessary and sufficient condition for the successful application of this approach was that the volume fractions did not change with deuterium content of the swelling solvents.

As was observed previously by others,[25] the fluid model, which incorporated length scales for the contrasting core and the radius of the hard-sphere interaction, did not completely account for the observed scattering at larger Q. There is an unaccounted length scale that required that we add an ad hoc second exponential function in addition to that assumed for the background function, $B(Q)$ (eq 1).

Figure 3 shows the results of nonlinear least-squares fits of the fluid model to the data obtained for Estane swollen in toluene mixtures. Figure 4a−c shows the fluid model fits to the data from the xylene isomers, and Figure 5 shows the fits obtained for the application of the fluid model with samples swollen in benzene. In each case the fluid model with the addition of the ad hoc exponential function reproduces the data.

There were no significant differences among the radii, R (from eqs 1 and 2), measured for the discrete domains, Φ', or D from samples swollen with either toluene or either of the xylene isomers as determined from the rms values of the fits (Supporting Information). Thus, Table 2 shows average values for many of the parameters, with the exception of the matrix phase compositions where there were significant differences. For these samples the detailed results are tabulated in the Supporting Information. Benzene, on the other hand, showed differences that were deemed significant due to the significantly greater uptake of solvent (Figure 2, Table 1), and these results are tabulated separately in Table 3.

For the toluene and xylene-swollen samples the average value of the radii (Table 2) was 4.82 nm, and the excluded volume radius, D, was 7.7 nm. The corresponding values were significantly larger for the benzene-swollen samples (Table 3) consistent with the relatively large presence of benzene. The hard-sphere excluded volume fraction, Φ', was 0.13 for all the solvents (Tables 2 and 3). From eq 3 we calculated that the discrete domain volume fraction was only about 0.03.

To obtain the information on domain composition, analysis of the contrast dependence of the Porod Invariant was used (eqs 11 and 12). Because Φ' was the same within the rms values of each of the toluene and xylene samples, we used the average value and the corresponding rms for all subsequent calculations. The assumption that the relevant scattering can be modeled as a solid sphere in the fluid model gave an analytical form to extrapolate the scattering of Q values to zero and to infinity for the purpose of calculating the integral in eq 4 and discounts any internal structure of the domains.

The Porod invariant, Q_p (Figure 6a), shows the expected parabolic dependence with ρ_{sol} (implied by the dependence of Q_p on the square of the contrast between the discrete domains and the matrix, eq 4). Figure 6b displays plots of $\sqrt{Q_p}$ vs ρ_{sol} for the various solvents, where the solid lines are the results of linear regression. The simple quadratic form of Q_p (Figure 6a) and the corresponding linear dependence of $\sqrt{Q_p}$ on ρ_{sol} (Figure 6b) are indicators that the requirement for this analysis that volume fractions determined using this analysis did not change with the amount of perdeuterated solvent was met.

The compositional information was obtained from the slope and the $Q_p = 0$ intercept as given by eqs 11 and 12. The toluene and xylene solvents show similar minima at $\rho_{sol} \sim 2.1 \times 10^{10}$ cm^{-2}. Thus, the volume fractions of the each component in the discrete domains φ_{im}, in the toluene and xylene swelling solvents did not differ by more than the uncertainties of the regression analysis; hence, we report the average values in Table 2. On the other hand, the benzene-swollen samples showed a lower solvent contrast match point, $\rho_{sol} = 1.8 \times 10^{10}$ cm^{-2}, indicating significant greater uptake of solvent in the discrete domains (Table 3). The compositional volume fractions for the matrix phase, φ_{iM}, were significantly different for each solvent, reflecting differences in the uptake in swelling solvent, ϕ_{sol} (Table 1), being almost entirely in the matrix phase (Tables 2 and 3).

According to the contrast variation analysis of the Porod invariant, the discrete domains largely excluded solvent, the values of φ_{Soli} not being significantly different from zero in all but the case of benzene (Tables 2 and 3) in which the discontinuous domain took up solvent to a volume fraction about 0.2. The estimated amount of soft segment in the discrete domains did not vary significantly among the swollen samples (Supporting Information); thus, we report the average of 0.53 for the soft segment volume fraction in the discrete domains (Table 2). This value was the same for benzene-swollen samples (Table 3). The hard segment content of the discrete domains, φ_{Hm}, was the same within the rms deviation of each determination for the toluene and xylene-swollen samples (Supporting Information) with an average volume fraction of 0.44 (Table 2). This value was significantly larger than that determined for the benzene-swollen sample (0.27).

The matrix took up the bulk of the solvent in all cases (Tables 2 and 3). This phase also contained both hard and soft segments, with about 0.1 of the volume fraction being hard segment in the toluene and xylene-swollen samples (Table 2). A somewhat smaller volume fraction of 0.068 was measured in the matrix phase of the samples swollen in benzene (Table 3) due to the significantly greater uptake of benzene. For the same reason the volume fraction of soft segment in the benzene-swollen samples were significantly less than with the other solvents (Tables 2 and 3). Given the total volume fraction of the matrix, most of the hard segment was in the matrix phase.

4.3. Micelle Model Analysis. For the micelle model, the data for each solvent contrast series were fit simultaneously. This allowed the compositional information to be obtained directly from the fits. That data for each contrast series could be fit simultaneously to the micelle model indicated that the structure and the content of the discrete domains and the matrix were not affected by the fraction of deuterium in the swelling agent. This is a more stringent condition than that required for the

Table 2. Average Domain Size and Composition of Estane Swollen in Toluene or One of the Xylene Isomers As Determined by the Fluid Model[a]

		matrix (M)			
phase	discrete domain (m) (averages)	toluene	*o*-xylene	*m*-xylene	*p*-xylene
Φ_j	0.032 ± 0.003[b]	0.97 ± 0.01[c]	0.97 ± 0.01[c]	0.97 ± 0.02[c]	0.96 ± 0.01[c]
R_m (nm)	4.82 ± 0.04				
N (cm^{-3})	$(6.9 \pm 0.7) \times 10^{16}$				
φ_{Hj}[d]	0.44 ± 0.04	0.093 ± 0.001	0.104 ± 0.001	0.101 ± 0.001	0.107 ± 0.002
φ_{Sj}	0.53 ± 0.07	0.386 ± 0.001	0.439 ± 0.001	0.442 ± 0.001	0.468 ± 0.001
φ_{solj}	0.01 ± 0.05	0.521 ± 0.001	0.457 ± 0.001	0.457 ± 0.001	0.425 ± 0.001

[a] Average hard-sphere radius $D = 7.7 \pm 0.2$ nm, and excluded volume fraction $\Phi' = 0.13 \pm 0.01$. [b] Discrete domain volume fraction, $1 - \Phi$. [c] Excluded region plus matrix volume fraction in swollen sample, Φ. [d] Subscript j equals m or M representing the discrete domain and matrix phase, respectively.

Table 3. Phase Dimensions and Composition of Estane Swollen by Benzene As Determined by the Fluid Model[a]

parameter	domain (m)	matrix (M)
Φ_j	0.03[b]	0.97 ± 0.02[c]
R_m (nm)	5.8 ± 0.4	
N (cm^{-3})	$(4.1 \pm 2.4) \times 10^{16}$	
φ_{Hj}[d]	0.27 ± 0.01	0.068 ± 0.001
φ_{Sj}	0.53 ± 0.01	0.284 ± 0.001
φ_{solj}	0.199 ± 0.005	0.648 ± 0.001

[a] Average hard-sphere radius $D = 9 \pm 3$ nm, and excluded volume fraction $\Phi' = 0.13 \pm 0.3$. [b] Discrete domain volume fraction, $1 - \Phi$. [c] Excluded region plus matrix volume fraction in swollen sample, Φ. [d] Subscript j equals m or M representing the discrete domain and matrix phase, respectively.

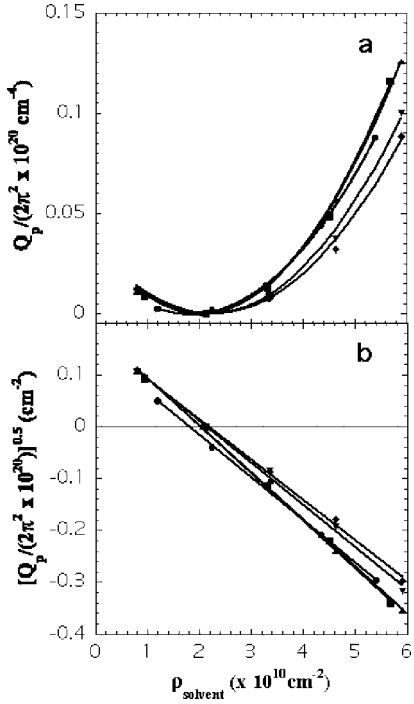

Figure 6. Contrast-dependent changes of Porod invariant for Estane swollen with either benzene, toluene, or either of the xylene isomers: (a) Porod invariant, Q_p, vs solvent scattering length density, $\rho_{solvent}$. (b) Square root of Q_p vs $\rho_{solvent}$. Data: samples swollen in (●) benzene, (▲) toluene, (■) *o*-xylene, (◆) *m*-xylene and (▼) *p*-xylene. Lines in Figure 5a are regression fits for Q_p to eq 4. Lines in Figure 5b are regression fits to the expected linear dependence of $\sqrt{Q_p}$ on $\rho_{solvent}$.

fluid model using the Porod invariant, which required that only the composition of the domains remain unaffected by f_D of the solvent. The sole exception was benzene, for which each member of the contrast series had to be fit separately.

We report the result from the toluene and either of the xylene-swollen samples as the average values in Table 4 with the individual results given in the Supporting Information and in Figures 2, 8, 9, and 10a,b. The results from the benzene-swollen samples are given in Table 5 and in Figures 2, 8, 9, and 10a,b.

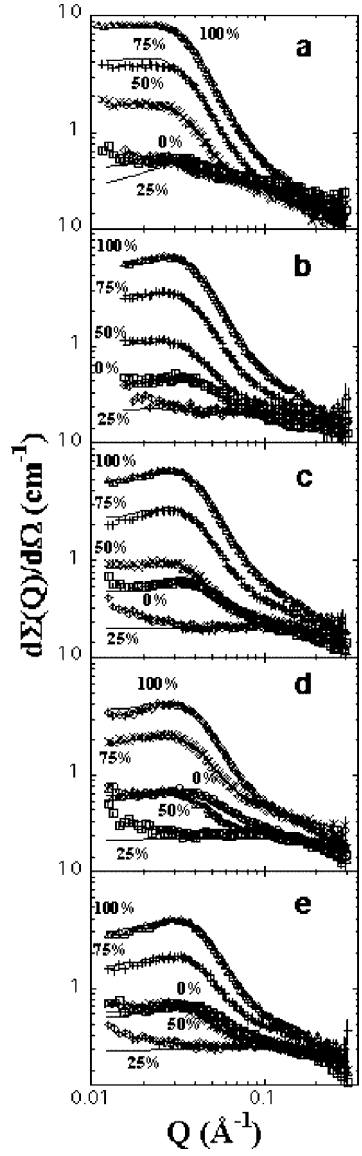

Figure 7. SANS of Estane swollen with mixtures of deuterated and protonated benzene, toluene, *o*-, *m*-, and *p*-xylene and comparison of the data with the *micelle* model: a: benzene; b: toluene, c: *o*-xylene; d: *m*-xylene; e: *p*-xylene. Data: Estane swollen in: (□) $f_D = 0$; (◇) $f_D = 0.25$; (×) $f_D = 0.50$; (+) $f_D = 0.75$; ρ, (△) $f_D = 1.0$. Small, vertical lines indicate the value of the standard deviation of the intensity data. Lines show the results of calculations for the micelle model.

The micelle model modeled the discrete domains as a core surrounded by a corona, providing an additional length scale not implicit in the fluid model. In the fitting process the volume fractions of the hard and soft segments in both the core and corona regions of the micelle were treated as free parameters. The remaining compositional parameters were calculated based

Table 4. Average Phase Size and Composition of Estane Swollen by Toluene or One of the Xylene Isomers As Determined by the Micelle Model[a]

	discrete domain (m)			
parameter	core (c)	corona (C)	core + corona (m)	matrix (M)
φ_j	$(4 \pm 2) \times 10^{-3}$	0.040 ± 0.006	0.039 ± 0.008[b]	0.956 ± 0.007[c]
R_j or T_C (nm)	2.5 ± 0.5	3.0 ± 0.1[d]	5.5 ± 0.5	
N (cm^{-3})			$(6.2 \pm 0.9) \times 10^{16}$	
φ_{Hj}	0.7 ± 0.1	0.13 ± 0.02	0.17 ± 0.01	0.116 ± 0.008
φ_{Sj}	0.3 ± 0.1	0.53 ± 0.04	0.51 ± 0.05	0.45 ± 0.05
φ_{solj}	0.02 ± 0.02	0.34 ± 0.06	0.31 ± 0.05	0.43 ± 0.05

[a] Average hard-sphere radius $D = 7.3 \pm 0.2$ nm, and excluded volume fraction $\Phi' = 0.100 \pm 0.007$. [b] Discrete domain volume fraction, $\Phi_m = 1 - \Phi$. [c] Hard-sphere excluded region plus matrix volume fraction in swollen sample, $\Phi_M = \Phi$. [d] Corona thickness, T_C.

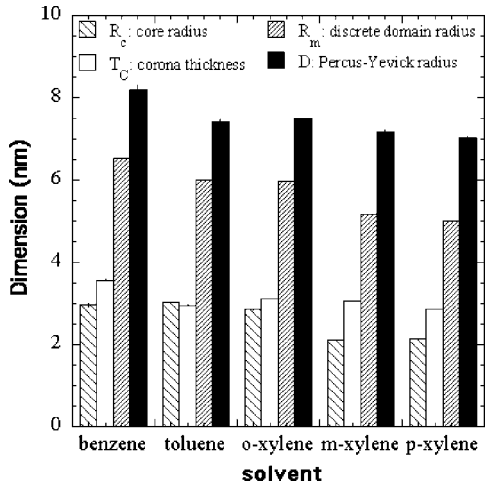

Figure 8. Domain dimensions in Estane swollen with mixtures of deuterated and protonated benzene, toluene, and *o*-, *m*-, and *p*-xylene.

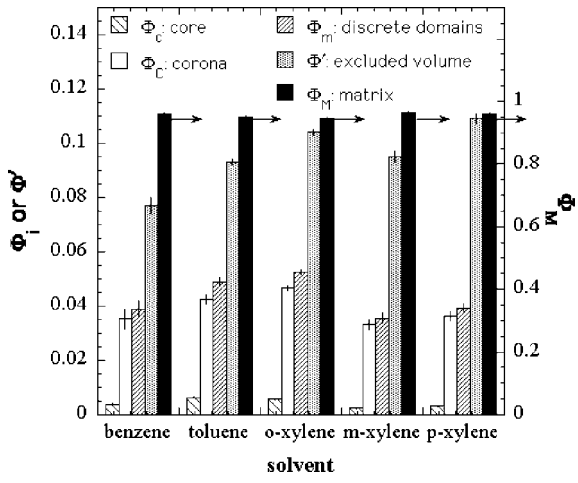

Figure 9. Domain volume fractions in Estane swollen with mixtures of deuterated and protonated benzene, toluene, and *o*-, *m*-, and *p*-xylene. Scale on right-hand axis is for Φ_M.

upon the best-fit values and the volume fraction constraints given in eqs 9 and 10, using the measured volume fractions listed in Table 1. The model largely accounted for the observed scattering (Figure 7), with the obvious exception of the low-Q region of the samples measured at low contrast where the scattering was dominated by sample nonhomogeneity. Thus, there was no need for additional ad hoc parameters as in the fluid model.

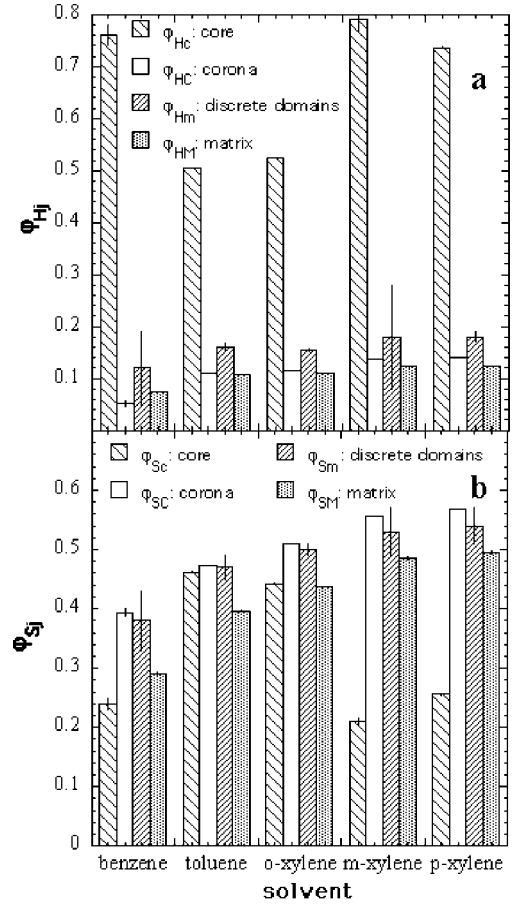

Figure 10. Hard and soft volume fractions in Estane domains swollen with mixtures of deuterated and protonated benzene, toluene, *o*-, *m*-, and *p*-xylene. (a) i = H, hard segment; (b) i = S, soft segment.

The parameters for the micelle model showed trends among the various solvents comparable to the analogous parameters of the fluid model. However, the rms values were substantially smaller for the micelle model in many cases. Thus, we discuss the results for the micelle model in greater detail.

The amount of solvent taken up in the cores of the discrete domains was zero or quite small (maximum $\varphi_{Solc} \approx 0.05$) (Figure 2), with an average value, $\overline{\phi_{Solc}} = 0.02 \pm 0.02$ (Figure 2 and Supporting Information) that was not significantly different from zero (Table 4). The solvent volume fractions in the corona and matrix (Figure 2) followed the same sequence observed for the total solvent uptake (Figure 2). However, the solvent volume fractions in the coronas were significantly smaller than those in the matrix (Figure 2), the difference among the solvents being fairly constant, 0.085 ± 0.005. The matrix solvent volume fractions were identical to the total solvent volume fractions taken up by the samples (Table 1 and Figure 2).

The average radius of the discrete domains, was found to be 5.5 ± 0.5 nm, very similar to the result obtained from fluid model. The trend for R_m and the thickness of the corona (Figure 8) was consistent with the amount of solvent taken up in the discrete domains, φ_{solm}, and corona, φ_{solC} (Figure 2). The hard-sphere exclusion radius, D (Figure 8), increased with the degree of solvent swelling (Figure 2). The number density of discrete domains decreased with increased swelling, with an average value of $(6 \pm 1) \times 10^{16}$ cm^{-3} (Supporting Information).

The volume fraction of each swollen domain, given in Figure 9, was fairly consistent with each solvent with no obvious correlations with swelling. The core accounted for an average of 0.004 ± 0.001 of the total volume, while the volume fraction of the discrete domain was 0.044 ± 0.007. The void volume

Table 5. Phase Dimensions and Composition of Estane Swollen by Benzene As Determined by the Micelle Model[a]

	discrete domain (m)			
parameter	core (c)	corona (C)	core + corona (m)	matrix (M)
φ_j	$(3.7 \pm 0.3) \times 10^{-3}$	0.035 ± 0.003	0.039 ± 0.003[b]	0.961 ± 0.003[c]
R_j or T_C (nm)	2.968 ± 0.004	3.562 ± 0.008[d]	6.530 ± 0.009	
N (cm^{-3})			$(4.64 \pm 0.02) \times 10^{16}$	
φ_{Hj}	0.76 ± 0.02	0.052 ± 0.006	0.12 ± 0.01	0.074 ± 0.001
φ_{Sj}	0.24 ± 0.01	0.394 ± 0.006	0.38 ± 0.05	0.291 ± 0.002
φ_{solj}	0.0 ± 0.03	0.55 ± 0.01	0.50 ± 0.06	0.635 ± 0.004

[a] Average hard-sphere radius $D = 8.2 \pm 0.1$ nm, and excluded volume fraction $\varphi' = 0.077 \pm 0.003$. [b] Discrete domain volume fraction, $\Phi_m = 1 - \Phi$. [c] Hard-sphere excluded region plus matrix volume fraction in swollen sample, $\Phi_M = \Phi$. [d] Corona thickness, T_C.

Table 6. Calculated Phase Composition and Size Derived from Estane Swollen in Either Benzene, Toluene, or One of the Xylene Isomers Corrected for Solvent Swelling Volume

	Fluid Model	
phase	discrete domain (m)	matrix (M)
Φ'_j	0.060 ± 0.009	0.94 ± 0.01
R'_m or D' (nm)	4.9 ± 0.3[a]	6.43 ± 0.08[b]
N' (cm^{-3})	$(1.18 \pm 0.07) \times 10^{17}$	
φ_{Hj}	0.43 ± 0.07	0.190 ± 0.004
φ_{Sj}	0.56 ± 0.07	0.81 ± 0.004

	Micelle Model			
phase	core (c)	corona (C)	Discrete domain (m)	matrix (M)
φ'_j	$(8 \pm 4) \times 10^{-3}$	0.045 ± 0.006	0.053 ± 0.009	0.947 ± 0.009
R'_j, T'_C, or D' (nm)	2.6 ± 0.5	2.6 ± 0.4[c]	4.9 ± 0.3[a]	6.0 ± 0.1[b]
N' (cm^{-3})			$(1.0 \pm 0.1) \times 10^{17}$	
φ_{Hj}	0.7 ± 0.1	0.18 ± 0.03	0.245 ± 0.008	0.204 ± 0.005
φ_{Sj}	0.3 ± 0.1	0.82 ± 0.03	0.75 ± 0.01	0.796 ± 0.005

[a] The discrete domain radius, R_m. [b] The Percus−Yevick excluded volume radius, D. [c] Corona thickness, T_C.

fraction, Φ', was found to have an average value of 0.10 ± 0.01.

As with the fluid model, discrete domains and matrix phase were found in the micelle model to be mixtures of hard and soft segments (Figure 10a,b and Supporting Information). The cores of the discrete domains contained primarily hard segment, $\overline{\phi_{Hc}} = 0.7 \pm 0.1$, with a corresponding average soft segment volume fraction over all the solvent-swollen samples, $\overline{\phi_{Sc}} = 0.3 \pm 0.1$. The volume fraction of hard and soft segments in the core varied significantly among the samples swollen with the different solvents (Figure 10a, Supporting Information) with no correlation with the overall amount of swelling. The corona that surrounds the core contained on average about 0.5 of its volume fraction as soft segment and a hard segment content that was similar to that found in the matrix phase (Figure 10a and Supporting Information). There was a decrease of the hard and soft segment volume fraction in the matrix phase as the solvent content increased (Figure 10a,b, Supporting Information). The matrix soft and hard segment content of the micelle model was (Table 4) consistent with the result of the fluid model (Table 2). The hard and soft segment content of the matrix phase of the micelle model was smaller with benzene (Table 5), again in agreement with the fluid model (Table 3) and consistent with the larger uptake of benzene.

5. Discussion

5.1. Estane Domain Morphology and Composition from Swelling Data. In order to estimate the structure and composition of neat, unswollen Estane (Table 6), we used the parameters in Tables 2–5 and Figures 7–10, correcting for the volume fraction taken up by the solvent. The various parameters in the swollen samples (Tables 2–5, Figures 7–10) should tend to agree with this correction, if volume occupied by the solvents was the only effect.

Indeed, this procedure brought many of the parameters derived for the different solvents into agreement. For example, for the fluid model volume-corrected values for R_m, Φ_m, Φ_M, φ_{HM}, and φ_{SM} (indicated by primes) were not significantly different from the averaged given in Table 6 for any of the solvents (Supporting Information). Furthermore, whereas the volume-corrected values from the fluid model discrete domain compositions, φ'_{Hm} and φ'_{Sm}, varied somewhat more from the average values (Table 6), this was not considered to be significant due to the relatively large rms values associated with these calculations (Supporting Information). Similarly for the micelle model the volume-corrected values for each solvent for R_m, R_c, T_C, φ_{HC}, φ_{SC}, φ_{Hm}, φ_{Sm}, φ_{HM}, and φ_{SM} were close to the average values in Table 6 (Supporting Information). The values of D', N', and Φ'_M, from the benzene, toluene, and xylene solvents, are close to the average values in Table 6 for both the fluid and micelle modes.

We concluded Estane is best described by the micelle model. The micelle consists of discrete spheroid domains with an average radius of ~5 nm and that these domains were best modeled as having a core, consisting of between 0.7 and 0.8 hard segment by volume, and a corona, consisting of approximately 0.18 hard segment and 0.82 soft segment by volume. The discrete domains were embedded in a matrix containing a hard segment volume fraction of ~0.2 and a soft segment volume fraction of 0.8 (Table 6), about the same composition as the bulk Estane (Table 1). The corona and matrix are not chemically distinct but were contrasted in these measurements, as the corona takes up significantly less solvent than the matrix (Figure 2). The discrete domain density was about 1.0×10^{17} cm^{-3}, corresponding to between 0.05 and 0.06 volume fraction of the sample, and had a most probable center-to-center distance of 13 and 12 nm according to the Percus−Yevick excluded volume analysis. These conclusions are based on the assumption that swelling does not affect the composition or morphology of the material, other than the volume increases that occur on swelling.

Koberstein and Leung[12,18] and Laity et al.[25] have also made determinations of the volume fraction of the discrete domains

in low (30 wt %) hard segment content of MDI-BDO-based poly(ether urethanes) analogous to Estane. Their estimates for the volume fraction of hard domains were 0.07[18] to 0.08[12] and 0.013,[25] respectively. Our values, when corrected for the volume fraction of solvent in the swollen samples, suggested volume fractions (Table 6) for the discrete domains in the neat Estane that were closer to those of Koberstein and Leung.[12,18]

The result that the soft segment-rich, matrix domain contains about 0.2 volume fraction of hard segment implies that 0.13 of the hard segment is in the discrete domains, as defined by the fluid model and 0.06 of the hard segment is in the discrete domains, as defined by the micelle model. According to the micelle model only 0.03 volume fraction of hard segment is in the discrete domain core; the only part of the Estane structure that is identifiable as consisting of mostly hard segment by swelling methods.

Our results provide additional information on the distribution of hard and soft segments into the structural domains of Estane, complementing the extensive work already in the literature.[1–21] In particular, the values for the volume fraction of hard segment in the discrete and continuous domains correspond well to that determined from thermal[19] and SAXS invariant[12,18] analysis of 30 wt % hard segment neat MDI-based poly(etherurethane), giving some validation of one key assumption of the analysis.

5.2. Phase Segregation and the Koberstein−Stein Model. The Koberstein−Stein model for segregation of hard segments into the hard and soft domains specified that the hard segments will phase separate when incorporated into a segment block (an *n*-mer) containing at least a critical number, N_c, of MDI monomers that are chemically linked in tandem by BDO extenders. Otherwise, the hard segments will be dissolved in the soft segment phase.[3,7,12] Koberstein and collaborators have estimated N_c to be 3−4[7] and 5−6[12] in various MDI-BDO-based poly(etherurethanes).

The statistical polymerization calculations of Peebles[50,51] showed that the fraction of MDI molecules in polyurethane chains that are present as *n*-mer hard segment blocks follows the most probable distribution, or the Schultz−Flory probability distribution

$$F_n = (1 - q)q^{n-1} \tag{13}$$

where q is the molar ratio of BDO to MDI (0.2:1.2) in the one-step reaction, assuming complete conversion. The prediction from this result is that the probability of finding an MDI in Estane as part of a dimer is 0.14. The fraction of MDI present in a trimer hard segment block is 0.023 and that likely to be present as part of a tetramer block is 0.004. The average size of the hard segment block is $(1 - q)^{-1} = 1.2$ MDI units. The fraction of MDI dimer blocks is in approximate agreement with an estimate of MDI dimer content of about 0.17 determined by integration of peaks measured in 2-dimensional $^{13}C-^{1}H$ NMR of Estane,[52] consistent with the prediction of the Pleebles model for the primary structure of Estane.

If we considered N_c as an average value for the minimum number of MDI units in the hard segment block needed to assemble as part of the discrete domains, then N_c may be taken to be a continuous variable analogous to n, which can be solved by inverting eq 13 using the fraction of hard segments incorporated into the discrete domains as an estimate for F_n. Using the procedure with F_n from the fluid model of 0.13 mole fraction of hard segments as being incorporated into the discrete domains gave $N_c = 2.0$, suggesting that incorporation into the discrete domains requires at least a dimer hard segment block. The fraction of hard segments in the discrete domains of the micelle model, 0.06, gave $N_c = 2.4$; thus, a mixture of dimer and trimer MDI blocks with a fraction of 0.4 trimers was needed to be incorporated into the discrete domains. The fraction of hard segments in the hard segment-rich core of the discrete domains of the micelle model, 0.03, keeping in mind that the corona is not chemically distinct from the matrix, gave a slightly larger value, $N_c = 2.8$. Thus, the fraction of trimers in the core was 0.8. All of these values were somewhat less than the lower end of Koberstein's estimates of the segregation criterion for some MDI-based poly(etherurethanes).[7,19] The discrete domains defined by the liquid and micelle models, while containing larger proportions of hard segments than the matrix, also contained a significant amount of soft segment, complicating the concept.

5.3. Estane Structure and Mechanical Properties. Measurements of Young's modulus, $E = 3G$ (assuming ideal rubber behavior, where Poisson's ratio = 0.5), gave 5 MPa[53] for Estane, giving $G = 1.7$ MPa. Simple network theory[54] gives the number of chains that extend from the cross-link, or the functionality, as $f = 2G/(k_B TN)$, where k_B is Boltzmann's constant. From the value of N' given in Table 6, $f \approx 8000$. Given the size and composition of the core of the discrete domains in the micelle model and assuming that each chain can visit the domain only once, we have a maximum plausible functionality of order 100. Thus, the notion that the discrete domains act solely as network cross-links requires an unphysically large functionality for the cross-links by at least 2 orders of magnitude.

The fraction of hard segment incorporated into the discrete domains implied that there was on average between 2.2 (micelle model) and 4.7 MDI (fluid model) incorporated into the discrete domains of the 37 or so MDI segments for the number-average molecular weight, W_n, of 45 kDa determined by column chromatography (GC, see methods) for the Estane chain, a value that is consistent with 40 kDa determined from NMR.[52] Our GC results (see methods) show that Estane has significant polydispersity with a PD of 1.8 (see methods). A Schulz−Zimm (SZ) distribution is expected for molecular weight distribution for the step polymerization used in Estane synthesis.[55] A SZ distribution consistent with our GC results ($M_n = 45$ kDa, $M_w = 81$ kDa, $M_z = 117$ kDa, and $M_w/M_n \equiv$ PD = 1.8) showed that a sizable fraction, 0.12, of the polymer population has a molecular weight at least twice that of N_n and 0.04 of the population is at least $3N_n$. Thus, the evidence obtained in this study pointed to the conclusion that there are no more than 1−2 connections to the discrete domains for the majority of polymer chains, arguing against these chains being able to participate in a network structure. However, some of the chains could have 2−4 or even more connections to the discrete domains and, thus, could plausibly be part of a network. It is beyond the scope of this paper to calculate the extent and probabilities of an extended network in this case.

If the majority of the chains are not likely to participate in a network, then coupling of the discrete domains would have to occur through entanglement with the matrix. Florez et al.[56] estimated the entanglement molecular weight of MDI-based polyesterurethanes with hexanediol and butanediol chain extenders for low hard segment content of 0.20 and 0.26 by weight as 2700 and 8500 Da, respectively. Considering these estimates were for the case where the molecular weight of the polyadipate is roughly twice that of the one used in Estane and that the methods used by Florez et al.[56] to measure the molecular weight likely gave an overestimate,[38] the values still indicated that the vast majority, about 0.95 for the SZ distribution above, of the chains are at or above the size at which they can become entangled.

One is struck by the observation that when small spheroid fillers were used to reinforce a polymer, the reinforcement achieved at 0.05 volume fraction of fillers, which interacted strongly with the polymer matrix, was similar to that obtained with 0.2 volume fraction filler that did not interact strongly.[57] This result was interpreted to be due, in part, to entanglement

Table 7. Flory−Huggins Interaction Parameters, χ, and Domain Moduli, G, Computed from Solubility Parameters and from Estane Swelling Data

			fluid model		micelle model[d] matrix		micelle model[d] corona	
solvent	χ_{SolS}[a]	χ_{SolH}[b]	χ'_{eff}[c]	G_M (MPa)	χ'_{eff}[c]	G_M (MPa)	χ'_{eff}[c]	G_C (MPa)
benzene	0.369	1.14	0.52	0.70	0.52	0.74	0.46	2.0
toluene	0.44	1.56	0.65	0.68	0.67	0.75	0.65	2.0
o-xylene	0.41	1.55	0.63	1.42	0.64	1.39	0.62	2.8
m-xylene	0.47	1.79	0.71	0.74	0.73	1.40	0.73	3.2
p-xylene	0.48	1.85	0.74	0.90	0.76	1.33	0.76	3.3

[a] χ_{SolH} is the Flory−Huggins interaction parameter for the soft segment with the solvents estimated using eq 16. [b] χ_{SolH} for the hard segment was computed from the δ values in Table 1 and from an estimate of the hard segment, $\delta = 23.5$ (MPa)$^{1/2}$. [c] χ'_{eff} is the volume fraction weighted average for the hard and soft segments (eq 15). [d] Values calculated from the matrix swelling data for the fluid (Tables 2 and 3) and the micelle (Table 5, Figure 2, and Supporting Information) models from eq 15 and eq 16.

between filler-bound polymer and the bulk polymer matrix, leading to coupling of the filler motion with the bulk polymer under stress.[57] Furthermore, a recent work considered mechanical models of the Young's modulus of different polyurethanes, including MDO-BDO based ones, with weight fraction of hard segment between 0.2 and 0.4, based on the concept of a filler volume fraction threshold of percolation.[58] The structure of polyurethanes was modeled as a rubbery matrix consisting entirely of soft segments filled by discrete domains consisting entirely of hard segments.[58] The segregation of the hard and soft segments and the volume fraction of "filler" used in the mechanical model was determined using a hard−soft segment Flory−Huggins interaction parameter calculated from estimates of the their solubility parameters. It was pointed out, however, the polyurtheanes is more complex than modeled by this relatively simple model filled system, as kinetic effects also determine the self-assembly into the different domains and hydrogen-bonding and crystallization effects come into play as well.[58]

5.4. Thermoelastic Aspects of Estane Swelling. The observation that the solvents swell the material to equilibrium provides a handle on the thermoelastic description of Estane swelling. The description of swelling was complicated by the domain structure of Estane and the observation that none of the domains are homogeneous. Regardless, the balance of factors governing swelling must apply to the system at equilibrium for each domain, *j*; thus, for each domain we assumed a simple, generalized Flory−Rehner form[30]

$$\ln \phi_{Solj} + (1 - \phi_{Solj}) + \chi'_{effj}(1 - \phi_{Solj})^2 + \frac{G_j V_s}{RT}(1 - \phi_{Solj})^{1/3} = 0 \quad (14)$$

where V_s is the solvent molar volume. Equation 14 reflects the balance of free energy of the entropy of ideal mixing in the absence of polymer−solvent interactions (two left-hand terms), solvent−polymer interactions, and deviations from ideal mixing (term in χ'_{effj}) and the work needed to swell the polymer (term in G_j) for each domain. An effective Flory−Huggins parameter, χ'_{effj}, is specified here to distinguish it from the single polymer−solvent interaction, χ, as χ'_{effj} should also include multiple interaction terms due to the heterogeneity of the polymer. In the absence of any other effects, we take χ'_{effj} to be the volume fraction-weighted average of the solvent interactions with the hard, χ_{SolH}, and soft segments, χ_{solS}

$$\chi'_{effj} = \phi'_{Hj}\chi_{SolH} + \phi'_{Sj}\chi_{SolS} \quad (15)$$

Table 7 tabulates χ_{SolS} values computed for the solvents and adipate soft segments, using the solubility parameters, δ, in Table 1 and the Shvarts relation[54]

$$\chi = \frac{V_s}{RT}(\delta_p - \delta_s)^2 + \chi_S \quad (16)$$

where δ_s is the solvent solubility parameter and R and T are the gas constant and temperature, respectively. Values for χ_{SolH} were calculated using eq 16 with an estimate for the hard segment solubility parameter of 23.5 (MPa)$^{1/2}$ (Table 7).[58,59] The entropic part of χ, χ_S, is estimated as 0.34 for both the hard and soft segments.[54] In eq 14 we have assumed that there is a specific modulus, G_j, associated with each domain and that the work done in swelling one domain had no effect on the work done of swelling another.

Sternstein[60] has developed a geometric, phenomenological theory for the micromechanics of swollen cross-linked elastomers around a spherical, included particle. The theory, which has been shown to be consistent with the interpretation of local birefringence measured by light scattering[61] and light microscopy,[62] predicts the strain components in the vicinity of the particle, one radial, λ_r, and the other tangential, λ_t. Both strain components vary with distance from the inclusion.[60] The λ_r component is a maximum at the particle interface and decreases monotonically with increasing distance from the particle, until it reaches the bulk matrix value, $\lambda_M = (1 - \phi_{SolM})^{-1/3}$. The $\lambda_t = 1$ at the particle interface and increases monotonically to λ_M. At the distance where the two strain components are equal, the strain field is isotropic and homogeneous, and eq 14 applies as written. However, within the domain where λ_r and λ_t vary, and this includes the corona region, it is likely that no single modulus describes the micromechanics. A detailed calculation of these moduli would require far more detail than was available from this study. Thus, G_C in eq 14 must be considered as an unspecified average of the anisotropic moduli over the entire corona region. G_C then describes the mechanical response of the corona as if it took up the solvent uniformly.

The estimates of χ from solubility parameters (Tables 1 and 7) indicated that neat adipate soft segment would swell indefinitely in all of the solvents, $\chi_{SolS} < 0.5$, whereas the MDI-BDO hard segments had very small swelling potential, $\chi_{SolH} > 1$ (Table 7). We included calculations in Table 7 using the swelling results from the fluid and micelle models to estimate χ'_{eff} using eq 15. The weighted average of these values suggested that overall $\chi'_{eff} > 0.5$ for the matrix domains of both models; thus, there was no need to invoke a network to account for equilibrium swelling in these samples. The same observation was seen for the corona domain, with the exception of the corona in benzene.

As crude as the above considerations were, they give some semiquantitative insight into the micromechanics of Estane domains through estimates of the local domain moduli, G_j, for the matrix domain from the fluid and micelle models and for the corona domain of the micelle model using eq 14. On the basis of these results the matrix domain, which represents the majority of the Estane volume, had for each solvent an estimated G value that was significantly smaller than the corresponding ones calculated for the corona domain of the matrix model (Table 7). According to the concepts implicit in eq 14, this result implied that the difference in swelling between the matrix and

corona was the result of the greater work needed to extend this domain. The Sternstein theory predicts our observation of an excess of polymer in the region of an inclusion and attributes this to complex strain gradients as described above.[60] Our observations then can be taken as qualitatively consistent with the strictly geometric, continuum theory of Sternstein at molecular lengths scales, much smaller than those measured previously.[61,62] However, the swelling characteristic of the corona was also a likely consequence of the constraints imposed by the corona's close association with the hard segment-rich core domain and the likelihood that the majority of the chains in this region are "tethered" to the core. Because of the nature of the approximations used in our calculations and the resulting semiquantitative nature of the results, the absolute values in Table 7 were not sufficiently accurate to make any further conclusions about the relationships between the *G* values in Table 7 and the measured bulk modulus.

Our statistical arguments, based on the relatively short number average of chain lengths and the relatively small probability of occurrence of hard segment dimers and trimers (that appear to meet the minimum requirement for incorporation into the discrete domains), suggest that there are relatively few discrete domains that are connected by the same polymer. This conclusion taken together with the observation that fillers with bound polymer entangled with the polymer matrix results in enhanced reinforcement[57] and the results of polyurethane mechanical modeling[58] leads to the hypothesis, that Estane largely behaves like a filled system highly coupled by entanglements to the embedding matrix by rubbery polymer segments anchored to the discrete domains in a manner analogous to the systems with polymer tethered to small, spheroid filler particles.

6. Conclusions

We demonstrated that swelling experiments using mixtures of deuterated and protonated solvents can be used in SANS measurements to determine the partitioning of the solvent among the different phases in a thermoplastic elastomer. Furthermore, the chemical composition size and distribution of the swollen phases can be determined by analyzing the data according to the method of contrast variation. Two models were considered, for analysis of the scattering data, the fluid and micelle models. Both models assumed the presence of spheroid, discrete domains in a continuous matrix. Of these, the micelle model, which assumed that the discrete domains consisted of a core surrounded by a corona, fit the data better than the fluid model, which assumed homogeneous, discrete domains. We found that the swelling agents, benzene, toluene, or *o*-, *m*-, and *p*-xylene, partitioned into the soft segment-rich matrix. Simple models of the scattering contrast suggested that in the matrix there is a significant amount of hard segment dissolved in the soft segment and that in the discrete domains there is a significant amount of soft segment mixed with hard segment. This conclusion is consistent with the results of earlier small-angle X-ray and NMR studies.

Acknowledgment. This work was supported by the US. Department of Energy at Los Alamos National Laboratory operated by the University of California under Contract W-7405-ENG-36 and subsequently by Los Alamos National Security LLC under Contract DE-AC52-06NA25396. This work benefited from the use of the Low-Q Diffractometer, LQD, at the Manuel Lujan, Jr. Neutron Scattering Center of the Los Alamos National Laboratory. We thank Joel Kress, David Hanson, Paul Welch, and Ed Kober of the Theoretical Division of Los Alamos National Laboratory for helpful discussions. We also acknowledge discussions with Cynthia Welch and Andrea Labouriau of the Materials Science and Technology Division of Los Alamos National Laboratory.

Supporting Information Available: Tables giving results of the analysis for each solvent used in this study. This material is available free of charge via the Internet at http://pubs.acs.org.

References and Notes

(1) Cooper, S. L.; Tobolsky, A. V. *J. Appl. Polym. Sci.* **1966**, *10*, 1837.
(2) Schneider, N. S.; Desper, C. R.; Illinger, J. L.; King, A. O.; Barr, D. *J. Macromol. Sci., Phys.* **1975**, *B11*, 527.
(3) Koberstein, J. T.; Stein, R. S. *J. Polym. Sci., Polym. Phys. Ed.* **1983**, *21*, 1439.
(4) Bonart, R.; Morbitizer, L.; Hentze, G. *J. Macromol. Sci., Phys.* **1969**, *B3*, 337.
(5) Van Bogart, J. W.; Gibson, P. E.; Cooper, S. L. *J. Polym. Sci., Polym. Phys. Ed.* **1983**, *21*, 65.
(6) Petrovic, Z. S.; Ferguson, J. *Prog. Polym. Sci.* **1991**, *16*, 695.
(7) Koberstein, J. T.; Galambos, A. F.; Leung, L. M. *Macromolecules* **1992**, *25*, 6195.
(8) Miller, J. A.; Lin, S. B.; Hwang, K. K. S.; Wu, K. S.; Gibson, P. E.; Cooper, S. L. *Macromolecules* **1985**, *18*, 32.
(9) Seefried, C. G.; Koleske, J. V.; Critchefield, F. E. *J. Appl. Polym. Sci.* **1975**, *19*, 2503.
(10) Wilkes, G. L.; Emerson, J. A. *Appl. Phys.* **1976**, *47*, 4261.
(11) Ryan, A. J.; Macosko, C. W.; Bras, W. *Macromolecules* **1992**, *25*, 6277.
(12) Koberstein, J. T.; Leung, L. M. *Macromolecules* **1992**, *25*, 6205.
(13) Li, C.; Goodman, S. L.; Albrech, R. M.; Cooper, S. L. *Macromolecules* **1988**, *21*, 2367.
(14) Miller, J. A.; Cooper, S. L.; Han, C. C.; Pruckmayr, G. *Macromolecules* **1984**, *17*, 1063.
(15) Cooper, S. L.; Miller, J. A., *Rubber Chem. Technol.* **1985**, *58*, 899.
(16) Garrett, J. T.; Runt, J.; Lin, J. S. *Macromolecules* **2000**, *33*, 6353.
(17) Cooper, S. L.; Miller, J. A. *Rubber Chem. Technol.* **1985**, *58*, 899.
(18) Leung, L. M.; Koberstein, J. T. *J. Polym. Sci., Polym. Phys. Ed.* **1985**, *23*, 1883.
(19) Leung, L. M.; Koberstein, J. T. *Macromolecules* **1986**, *19*, 706.
(20) Wilkes, G. L.; Wildnauer, R. *J. Appl. Phys.* **1975**, *46*, 4149.
(21) Nierzwick, W.; Majewska, Z. *J. Appl. Polym. Sci.* **1979**, *24*, 1089.
(22) Li, Y.; Fao, T.; Chu, B. *Macromolecules* **1992**, *25*, 1737.
(23) Clayden, N. J.; Nijs, C.; Eeckhaut, G. *Macromolecules* **1998**, *31*, 7820.
(24) Krakovsky, I.; Bueniková, Z.; Urakawa, H.; Kajiwara, K. *Polymer* **1997**, *38*, 3637.
(25) Laity, P. R.; Taylor, J. E.; Wong, S. S.; Khunkamchoo, P.; Norris, K.; Cable, M.; Andrews, G. T.; Johnson, A. F.; Cameron, R. E. *Polymer* **2004**, *45*, 7273.
(26) Oberth, A. E. *Rubber Chem. Technol.* **1990**, *63*, 56.
(27) Kobayashi, M.; Yoshioka, T.; Imai, M.; Itoh, Y. *Macromolecules* **1995**, *28*, 7376.
(28) Geissler, E.; Harkay, F.; Hecht, A.-M.; Roches, C.; Lindner, P.; Bourgaux, C.; Couarraze, G. *Polymer* **1997**, *38*, 15.
(29) Horkay, F.; Hecht, A.-M.; Geissler, E. *Macromolecules* **1998**, *31*, 8851.
(30) Flory, P. J.; Rehner, J. *J. Chem. Phys.* **1943**, *11*, 521.
(31) Gumbrell, S. M.; Mullins, L.; Rivlin, R. S. *Trans. Faraday Soc.* **1953**, *49*, 1495.
(32) Aithal, U.S.; Aminabhavi, T. M.; Balungi, R. H.; Shukla, S. S. *J. Macromol. Sci., Rev. Macromol. Chem. Phys* **1990**, *C30*, 43.
(33) Hjelm, R. P. *Am. Chem. Soc. Symp.* **2002**, *804*, 71.
(34) Hjelm, R. P.; Wampler, W. A.; Seeger, P. A.; Gerspacher, M. *J. Mater. Res.* **1994**, *9*, 3210.
(35) Hjelm, R. P.; Wampler, W. A.; Gerspacher, M. *Mater. Res. Soc. Symp. Proc.* **1996**, *376*, 303.
(36) Espada, L. I.; Mang, J. T.; Orler, E. B.; Wrobleski, D. A.; Langlois, D. A.; Hjelm, R. P. *Polym. Prepr.* **2001**, *42*, 693.
(37) Hoffman, D. M.; Caley, L. E. *ACS Div. Org. Coat. Plast. Chem.* **1981**, *44*, 686.
(38) Wrobleski, D. A.; Orler, E. B.; Smith, M. E. *Polym. Prepr.* **2001**, *42*, 669.
(39) Hjelm, R P. *J. Appl. Crystallogr.* **1988**, *21*, 858.
(40) Seeger, P.; Hjelm, R P. *J. Appl. Crystallogr.* **1991**, *24*, 467.
(41) Petersen, J. S. *J. Appl. Crystallogr.* **2000**, *33*, 637.
(42) Pedersen, J. S.; Hamley, I. W.; Ryu, C. Y.; Lodge, T. P. *Macromolecules* **2000**, *33*, 542.
(43) Arleth, L.; Bashok, B.; Onyuksel, H.; Thiyagarajan, P.; Jacob, J,.; Hjelm, R. P. *Langmuir* **2005**, *21*, 3279.
(44) Ashcroft, W.; Lekner, J. *Phys. Rev.* **1966**, *145*, 83.
(45) Kinning, D. J.; Thomas, E. L. *Macromolecules* **1984**, *17*, 1712.
(46) Stuhrmann, H. B.; Duee, E. D. *J. Appl. Crystallogr.* **1975**, *8*, 538.
(47) Stuhrmann, H. B.; Haas, J.; Ibel, K.; Koch, M. H. J.; Crichton, R. R. *J. Mol. Biol.* **1976**, *100*, 399.
(48) Hoy, K. L. *J. Paint Technol.* **1970**, *42*, 76.
(49) Hawley, M. E.; Orler, E. B.; Wrobleski, D. A.; Hjelm, R. P.; Brown, G. W. *Mater. Res. Soc. Symp. Proc.* **2001**, *661*, KK4.7.1.
(50) Peebles, L. H. *Macromolecules* **1974**, *7*, 872.

(51) Peebles, L. H. *Macromolecules* **1976**, *9*, 58.
(52) Lemaster, D. M.; Hernández, G. *Macromolecules* **2000**, *33*, 3569.
(53) Banergee, B.; Cady, C. M.; Adams, D. O. *Modelling Simul. Mater. Sci. Eng.* **2003**, *11*, 457.
(54) Treloar, L. R. G. *The Physics of Rubber Elasticity*, 3rd ed.; Oxford University Press: New York, 1975.
(55) Strobl, G. *The Physics of Polymers*, 2nd ed.; Springer: New York, 1997.
(56) Florez, S.; Muñoz, E.; Santamaría, A. *J. Rheol.* **2005**, *49*, 313.
(57) Sternstein, S. S.; Zhu, A.-J. *Macromolecules* **2002**, *35*, 7262.
(58) Ginzburg, V. V.; Bicerano, J.; Christenson, C. F.; Schrock, A. K. *J. Polym. Sci., Part B: Polym. Phys.* **2007**, 2124.
(59) Ryan, A. J.; Stanford, J. L.; Hill, R. H. *Polym. Commun.* **1988**, *29,* 196.
(60) Sternstein, S. S. *J. Macromol. Sci., Phys.* **1972**, *B6*, 243.
(61) Picot, C.; Fukuda, M.; Chou, C.; Stein, R. S. *J. Macromol. Sci., Phys.* **1972**, *B6*, 263.
(62) Kotani, T.; Sternstein, S. S. In *Polymer Networks: Structure and Mechanical Properties*; Chompff, A. J., Newman, S., Eds.; Plenum Press: New York, 1971.

MA800015G